ChemComm

COMMUNICATION

View Article Online
View Journal | View Issue

Cite this: *Chem. Commun.*, 2018, **54**, 3247

Received 2nd February 2018,
Accepted 16th February 2018

DOI: 10.1039/c8cc00933c

rsc.li/chemcomm

A synthesis-enabled relative stereochemical assignment of the C1–C28 region of hemicalide†

Bing Yuan Han,‡ Nelson Y. S. Lam,‡ Callum I. MacGregor, Jonathan M. Goodman and Ian Paterson*

Through synthesising both candidate diastereomers of a model C1–C28 fragment of the potent cytotoxic marine polyketide hemicalide, an assignment of the relative configuration between the C1–C15 and C16–C26 regions has been achieved. By detailed NMR comparisons with the natural product, the relative stereochemistry between these two 1,6-related stereoclusters is elucidated as 13,18-*syn* rather than the previously proposed 13,18-*anti* relationship. A flexible and modular strategy using an advanced C1–C28 ketone fragment 22 is outlined to elucidate the remaining stereochemical features and achieve a total synthesis.

Extracted from the marine sponge *Hemimycale* sp., hemicalide (**1**, Fig. 1) was reported to display impressive picomolar IC_{50} values against a panel of human cancer cell lines. Initial studies pointed towards a novel antimitotic mechanism of action *via* microtubule destabilisation, but its low isolation yield (0.5 mg) precluded further biological evaluation.[1] While extensive 1D and 2D-NMR experiments were able to ascertain the planar structure of hemicalide, the paucity of material rendered its full 3D structural elucidation elusive. Indeed, all 21 stereocentres were left unassigned in the patent application, leading to over 2 million possible permutations.

Through a combination of computational NMR shift predictions and spectroscopic corroboration from synthesised model fragments, we, together with the Ardisson and Cossy/Meyer groups, have assigned the relative configuration of hemicalide for the C8–C13 stereohexad **2**,[2,3] C16–C26 dihydroxylactone **3**[4,5] and C35–C42 hydroxylactone **4**.[6] To date, the relative and absolute configuration of the C26–C34 polyacetate region, and the isolated C45 stereocentre remained unassigned.[6] While efforts have been reported by the Ardisson and Cossy/Meyer groups towards joining the fragments together, previously reported synthetic studies on the full C1–C27 fragment have targeted the 13,18-*anti* diastereomer **5a**;[5,7] only one of the two diastereomeric possibilities between the C1–C15 and the C16–C26 regions. Through the synthesis and detailed NMR spectroscopic comparisons of

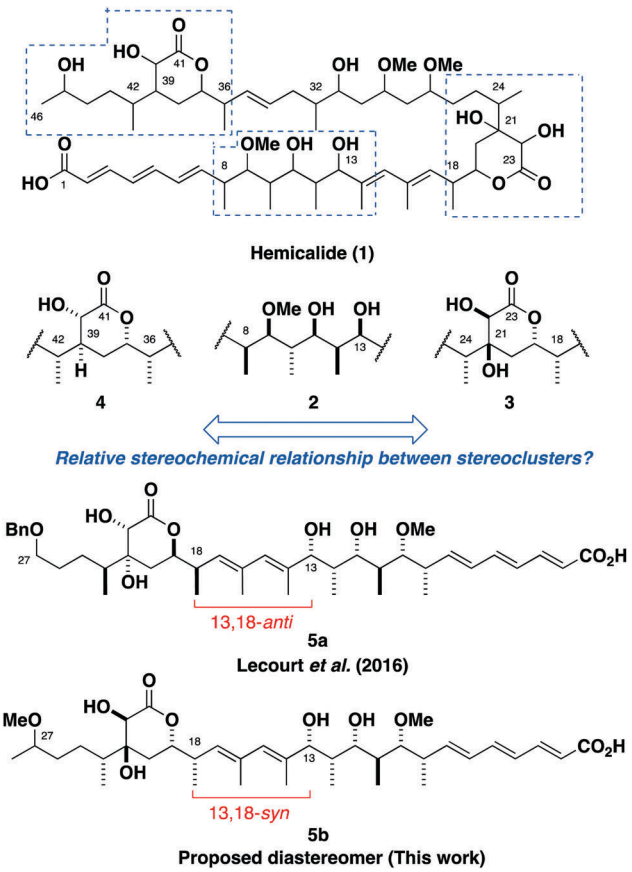

Fig. 1 The planar structure for hemicalide (**1**) and the assigned relative configurations of each subunit.[2–4,6] Previous endeavours towards the total synthesis of hemicalide have targeted the 13,18-*anti* diastereomer **5a**. This work reassigns the relative configuration to be as represented in the 13,18-*syn* diastereomer **5b**.

University Chemical Laboratory, Lensfield Road, Cambridge, CB2 1EW, UK. E-mail: ip100@cam.ac.uk

† Electronic supplementary information (ESI) available: Full experimental and characterisation details; NMR correlation tables and bar graphs. See DOI: 10.1039/c8cc00933c

‡ Authors contributed to this manuscript equally.

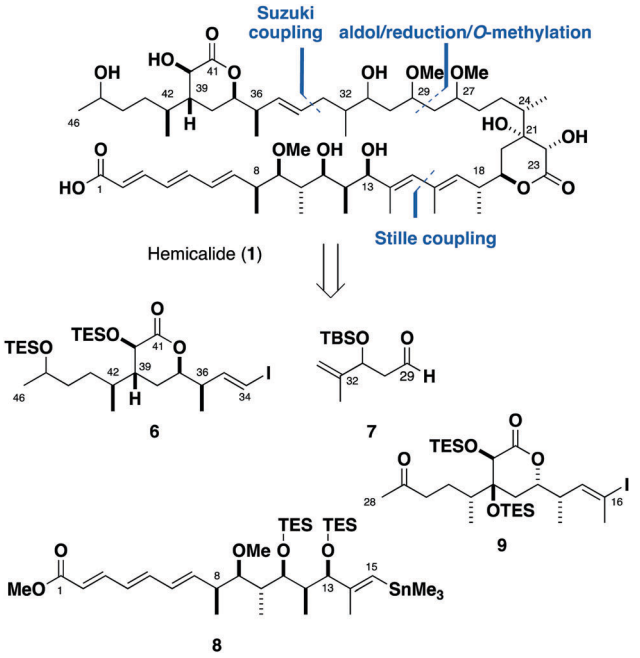

Scheme 1 Retrosynthetic analysis of hemicalide (**1**) reveals key fragments **6–9**. Note that only the relative configuration within each of the three stereoclusters is suggested.

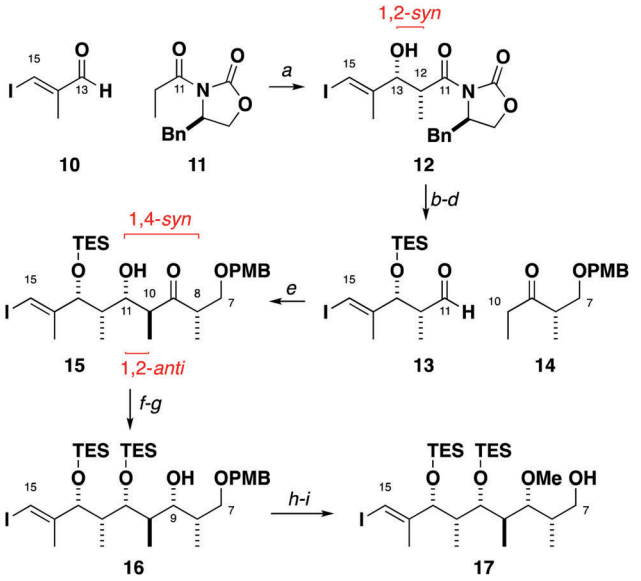

Scheme 2 Synthesis of hemicalide fragment **17**. *Reagents and conditions*: (a) **11**, Bu_2BOTf, DIPEA, 0 °C; **10**, −78 °C to −20 °C, 83%; (b) TESCl, imidazole, r.t., 99%; (c) $LiBH_4$, 0 °C, 65%; (d) $(COCl)_2$, DMSO, Et_3N, −78 °C to −20 °C, 99%; (e) **14**, *c*-Hex_2BCl, Et_3N, 0 °C; **13**, −78 °C to −20 °C, 65%; (f) TESOTf, 2,6-lutidine, −78 °C, 70%; (g) DIBAL, −40 °C, 70%; (h) $Me_3O{\cdot}BF_4$, Proton Sponge®, 4 Å MS, r.t., 72%; (i) DDQ, CH_2Cl_2, pH 7 buffer, 0 °C to r.t., 99%.

both candidate diastereomers, we herein report the likely relative configuration of the full C1–C28 region of hemicalide as in the 13,18-*syn* diastereomer **5b**.

Our approach needed to be modular and highly stereoselective to allow for the facile synthesis of both enantiomers of each fragment. Given that the majority of the missing stereochemical information lies in the C27–C34 region, a flexible strategy was devised involving a late stage aldol/reduction sequence to forge the C27 and C29 stereocentres (Scheme 1). A cross-coupling was envisaged to connect the C34–C46 hydroxylactone **6** with each enantiomer of the C29–C33 aldehyde **7**, as well as the C1–C15 and C16–C28 fragments **8** and **9** together.

Our first quest towards determining the complete stereochemistry of hemicalide began with the C1–C28 region, consisting of the C1–C15 and the C16–C28 stereoclusters. With computational methods proving useful in elucidating the relative configuration within the isolated fragments,[2,4] we initially sought to employ our DP4f methodology[2] to elucidate their relative stereochemical relationship. However, due to the size and flexibility of the virtual fragments involved, it proved to be too computationally demanding to accurately model the C1–C28 truncate. As such, we turned towards synthesising both candidate diastereomers of the full C1–C28 region to elucidate the relative configuration between these two stereoclusters. We envisioned that meaningful NMR differences could be observed for each diastereomer despite the relatively remote 1,6-related chiral environments between C13 and C18 adjacent to the connecting *E,E*-diene.[8]

The stereohexad in the C1–C15 region **8** was installed by asymmetric boron-mediated aldol reactions. Starting from aldehyde **10**, an Evans aldol reaction (Bu_2BOTf, DIPEA)[9] with oxazolidinone **11** gave adduct **12** as a single diastereomer, setting up the 1,2-*syn* relationship at C12 and C13 (Scheme 2). TES protection and auxiliary cleavage ($LiBH_4$) followed by a Swern oxidation gave aldehyde **13**. Using our standard conditions (*c*-Hex_2BCl, Et_3N),[10] ethyl ketone **14** was engaged with aldehyde **13** to yield the 1,2-*anti*-1,4-*syn* adduct **15** (>20 : 1 dr). The C11 hydroxyl group was TES protected before submitting to a controlled reduction (DIBAL) to afford alcohol **16** (>20 : 1 dr, see the ESI† for confirmation of stereochemistry). Methylation ($Me_3O{\cdot}BF_4$, Proton Sponge®) and deprotection of the PMB ether (DDQ) gave **17**. As the absolute configuration is set by **11** and **14**, the enantiomer of **17** was obtained in a similar fashion by employing **ent-11** and **ent-14** instead.

The phosphonate **18** (Scheme 3) was prepared in three steps from sorbic acid. We previously reported in the enantiomeric series the synthesis of the C16–C28 ketone **9** in 16 steps from aldehyde **19**.[4] Dess–Martin oxidation of alcohol **17** provided aldehyde **20**, which was subjected to an HWE olefination with phosphonate **18** to afford the C1–C15 vinyl iodide as a single geometric isomer. At this juncture, the planned cross-coupling step required the appendage of a stannane handle onto either the C1–C15 or the C16–C28 vinyl iodide (**21** and **9** respectively). As the C16 vinyl stannane proved to be highly prone to decomposition, we instead converted the vinyl iodide **21** to the corresponding stannane **8** under Wulff–Stille conditions ($Pd(PPh_3)_2Cl_2$, $(Me_3Sn)_2$).[11] With the two key fragments in hand, a modified Stille coupling[12] afforded the advanced C1–C28 ketone **22**. By repeating the Stille coupling with **ent-8**, the 13,18-*anti* diastereomer **23** was also obtained in an analogous manner. Encouragingly, NMR comparisons in $CDCl_3$ indicated clear differences between the

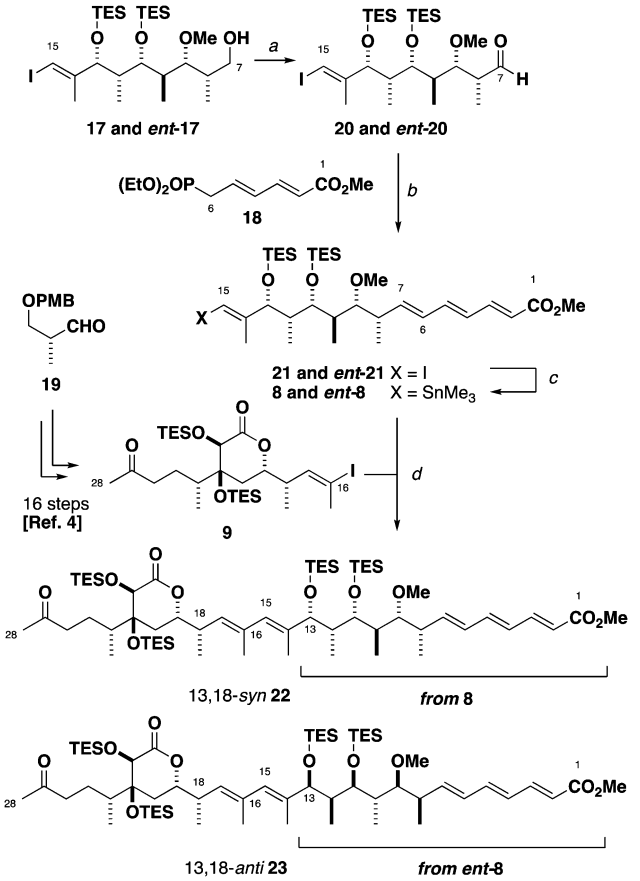

Scheme 3 Synthesis of hemicalide fragments **22** and **23**. *Reagents and conditions*: (a) DMP, $NaHCO_3$, CH_2Cl_2, 0 °C to r.t., 99%; (b) LDA, **20**, −78 °C; **18**, −78 → −20 °C, 65%; (c) $(Me_3Sn)_2$, $Pd(PPh_3)_2Cl_2$ (10 mol%), Li_2CO_3, DMF, 80 °C, 70%; (d) $Pd(PPh_3)_4$ (20 mol%), CuTC, DMF, 0 °C, 72%.

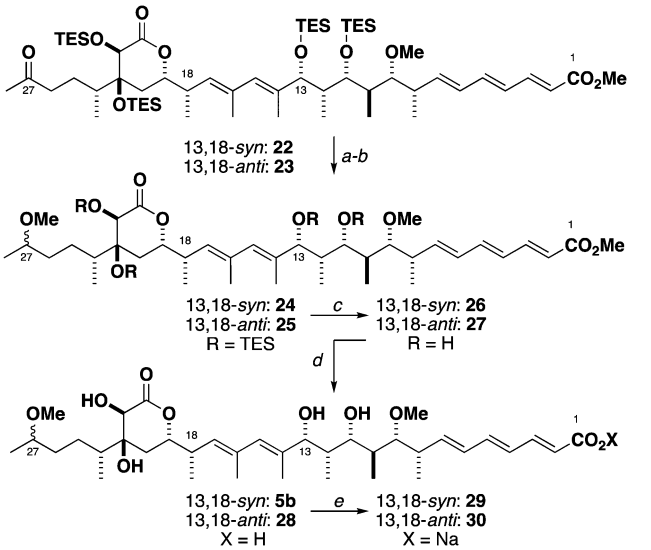

Scheme 4 Synthesis of model fragments for NMR comparison. *Reagents and conditions*: (a) $NaBH_4$, MeOH, 95%; (b) $Me_3O{\cdot}BF_4$, Proton Sponge®, 4 Å molecular sieves, CH_2Cl_2, 87%; (c) TASF, THF/DMF, 0 °C *then* HF·py/py, THF, 0 °C, 95% over two steps; (d) $Ba(OH)_2{\cdot}8H_2O$, MeOH, 50%; (e) Na_2CO_3, d_4-MeOD, 99%.

protected 13,18-*syn* and 13,18-*anti* diastereomers despite the distal nature of the two stereoclusters.

Initial exploratory studies showed that deprotecting the C16–C28 ketone resulted in the concomitant hemiacetal engagement with the C27 carbonyl. Furthermore, the natural product contains a methyl ether at C27 and its presence is expected to aid a more representative NMR correlation. As such, we looked to transform the C27 carbonyl to the corresponding methyl ether. Attempts at effecting a stereoselective reduction on both the full truncate, as well as the C16–C28 lactone and intermediates thereof proved to be ineffective. Guided by previous reports[6] that the configuration of the distal C46 hydroxyl group had little influence with NMR shifts on the C36–C46 fragment, we separately subjected **22** and **23** to a non-selective reduction ($NaBH_4$) and methylation ($Me_3O{\cdot}BF_4$, Proton Sponge®) to afford the C27 methyl ethers **24** and **25** (Scheme 4). While the C27 epimers were inseparable by chromatography, the NMR assignment proved to be straightforward. Global silyl deprotection was found to be problematic. After extensive experimentation, careful treatment of the protected model truncates with TASF followed by HF·py/py reliably afforded tetraols **26** and **27**. Ester hydrolysis using $Ba(OH)_2$[13] provided the acids **5b** and **28**.

We found that the NMR chemical shifts for the C1–C7 region were highly dependent on the protonation state of the C1 carboxylic acid (see the ESI†), though this did not appear to significantly affect the signals for the remainder of the molecule. The effect of the protonation state on the ^{13}C NMR was most noticeable for C1–C3, where presumed proton exchange kinetics resulted in peak broadening in acids **5b** and **28**. To verify this hypothesis, and noting that the natural product was proposed to be isolated as the carboxylate salt,[3] *in situ* treatment of the free acid with Na_2CO_3 effected complete acid deprotonation, which sharpened the carbon signals at C1-C3 in the sodium salts **29** and **30**.

At this stage, we were able to compare both the ^1H and ^{13}C NMR chemical shifts of our model truncates **5b** and **28** with the 13,18-*anti* truncate **5a** of Lecourt *et al.*[5] and hemicalide itself. Notably the 13,18-*anti* acid **28** correlated well with the spectroscopic data reported for **5a** (see the ESI†). The differences did not appear to be particularly diagnostic in the ^1H NMR spectra for both acids **5b** and **28**, however, distinct differences were noted when comparing their ^{13}C NMR data to the natural product (Fig. 2).[1] In particular, the chemical shift differences for the 13,18-*syn* acid **5b** did not exceed ±0.01 ppm for ^1H NMR, and ±0.1 ppm for ^{13}C NMR. This was in contrast to the 13,18-*anti* acid **28**, where differences up to ±0.04 ppm (H11) and ±0.6 ppm (C11) were observed for the ^1H and ^{13}C NMR shifts respectively. Overall, the absolute and maximum errors recorded for the 13,18-*syn* diastereomers (Table 1, entries 1 and 2) were noticeably smaller than the corresponding 13,18-*anti* diastereomers (Table 1, entries 4 and 5) and to previously published values for **5a** (entry 3).[5] Interestingly, while the natural product was proposed to be isolated as the carboxylate salt,[3] the correlation for both diastereomers of salts **29** and **30** (entries 2 and 5) was poorer than for the corresponding acids **5b** and **28** (entries 1 and 4), particularly in the C1–C7 triene region (see the ESI†). This suggests that hemicalide was likely isolated as the acid rather than the carboxylate salt.

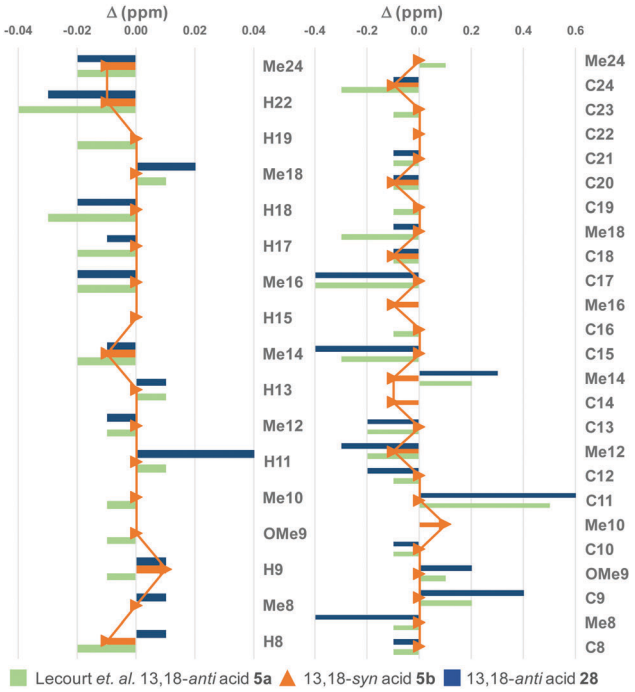

Fig. 2 Bar graph highlighting the ^{1}H (left) and ^{13}C (right) NMR chemical shift differences between the model acids and hemicalide (**1**) between H8/C8 and Me24, overlaid with a line graph for acid **5b**. ^{1}H signals contained within the 22H multiplet in the natural product are omitted for comparison. See the ESI† for expanded bar graphs comparing acids **5a**, **5b**, **28** with salts **29** and **30**.

Table 1 Sum of absolute errors |Δ| (ppm)[a,b] for each diastereomer compared to the reported spectra of **1**[1]

Entry		Sum |Δ| ^{1}H	Max |Δ| ^{1}H	Sum |Δ| ^{13}C	Max |Δ| ^{13}C
1	13,18-*syn* acid **5b**	**0.05**	**0.01**	**0.8**	**0.1**
2	13,18-*syn* salt **29**	0.08	0.02	1.7	0.2
3	Lecourt *et al.* acid **5a**	0.26	0.04	3.8	0.5
4	13,18-*anti* acid **28**	0.22	0.04	4.1	0.6
5	13,18-*anti* salt **30**	0.22	0.04	4.3	0.7

[a] Absolute errors taken for NMR shifts between C8–Me24. [b] |Δ| = δ(experimental shift) – δ(reported shift), errors in ppm.

In conclusion, we have firmly established the relative configuration between the C8–C13 and C16–C24 stereoclusters in hemicalide, where NMR correlations of advanced fragments decisively supported the reassigned 13,18-*syn* relationship. Additionally, NMR comparisons in the C1–C7 triene region indicated that hemicalide was likely isolated as the acid rather than the carboxylate salt. Our highly flexible construction of the advanced C1–C28 ketone **22** also enables the synthesis of the enantiomer **ent-22**. We hope to then achieve a bioassay-guided determination of hemicalide's absolute configuration, as well as ascertaining preliminary structure–activity relationships in a drug development context.[14]

We thank the Woolf Fisher Trust (NYSL), the EPSRC (CIM) for financial support and the National Mass Spectrometry Centre (Swansea) for mass spectra.

Conflicts of interest

There are no conflicts to declare.

Notes and references

1 I. Carletti, C. Debitus and G. Massiot, *Molécules polykétides comme agents anticancéreux*, *Pat. Appl. Pub.*, WO2011051380A1(FR), 2011 (*Chem. Abstr.*, 2011, **154**, 5130950).
2 S. G. Smith and J. M. Goodman, *J. Am. Chem. Soc.*, 2010, **132**, 12946.
3 E. Fleury, M.-I. Lannou, O. Bistri, F. Sautel, G. Massiot, A. Pancrazi and J. Ardisson, *J. Org. Chem.*, 2009, **74**, 7034.
4 C. I. MacGregor, B. Y. Han, J. M. Goodman and I. Paterson, *Chem. Commun.*, 2016, **52**, 4632.
5 C. Lecourt, S. Boinapally, S. Dhambri, G. Boissonnat, C. Meyer, J. Cossy, F. Sautel, G. Massiot, J. Ardisson, G. Sorin and M.-I. Lannou, *J. Org. Chem.*, 2016, **81**, 12275.
6 S. Specklin, G. Boissonnat, C. Lecourt, G. Sorin, M.-I. Lannou, J. Ardisson, F. Sautel, G. Massiot, C. Meyer and J. Cossy, *Org. Lett.*, 2015, **17**, 2446.
7 G. Sorin, E. Fleury, C. Tran, E. Prost, N. Molinier, F. Sautel, G. Massiot, S. Specklin, C. Meyer, J. Cossy, M.-I. Lannou and J. Ardisson, *Org. Lett.*, 2013, **15**, 4734.
8 I. Paterson, S. M. Dalby, J. C. Roberts, G. J. Naylor, E. A. Guzmán, R. Isbrucker, T. P. Pitts, P. Linley, D. Divlianska, J. K. Reed and A. E. Wright, *Angew. Chem., Int. Ed.*, 2011, **50**, 3219.
9 D. A. Evans, J. Bartroli and T. L. Shih, *J. Am. Chem. Soc.*, 1981, **103**, 2127.
10 I. Paterson, G. J. Florence, K. Gerlach, J. P. Scott and N. Sereinig, *J. Am. Chem. Soc.*, 2001, **123**, 9535.
11 W. D. Wulff, G. A. Peterson, W. E. Bauta, K.-S. Chan, K. L. Faron, S. R. Gilbertson, R. W. Kaesler, D. C. Yang and C. K. Murray, *J. Org. Chem.*, 1986, **51**, 277.
12 A. Fürstner, J.-A. Funel, M. Tremblay, L. C. Bouchez, C. Nevado, M. Waser, J. Ackerstaff and C. C. Stimson, *Chem. Commun.*, 2008, 2873.
13 I. Paterson, K. S. Yeung, R. A. Ward, J. G. Cumming and J. D. Smith, *J. Am. Chem. Soc.*, 1994, **116**, 9391.
14 For related recent work from our group, see: (*a*) I. Paterson and N. Y. S. Lam, *J. Antibiot.*, 2018, **71**, 215; (*b*) N. Anžiček, S. Williams, M. P. Housden and I. Paterson, *Org. Biomol. Chem.*, 2018, DOI: 10.1039/c7ob03204h.

